Electronic Supporting Information

A rational study of the influence of Mn^{2+}-insertion in Prussian blue nanoparticles on their photothermal properties

Maëlle Cahu,[a&] Lamiaa M.A. Ali,[b,c&] Saad Sene,[a] Jérôme Long,[a] Franck Camerel,[d] Mathieu Ciancone,[d] Fabrice Salles,[a] Joël Chopineau,[a] Jean-Marie Devoisselle,[a] Gautier Felix,[a] Nicolas Cubedo,[e] Mireille Rossel,[e] Yannick Guari,[a] Nadir Bettache,[b] Joulia Larionova,[a,*] Magali Gary-Bobo[b*]

[a]*ICGM, Univ. Montpellier, CNRS, ENSCM. Montpellier, France. E-mail : joulia.larionova@umontpellier.fr*

[b]*IBMM, Univ. Montpellier, CNRS, ENSCM. Montpellier, France. E-mail: magali.gary-bobo@inserm.fr*

[c]*Department of Biochemistry, Medical Research Institute, University of Alexandria, Alexandria, Egypt.*

[d]*Univ Rennes, ENSCR, CNRS, ISCR (Institut des Sciences Chimiques de Rennes) - UMR 6226, 35000 Rennes, France*

[e] *MMDN, Univ Montpellier, EPHE, PSL, INSERM, Montpellier, F-34095 France*

[&] *These authors contributed equally to this work*

Table S1. Relevant characteristics of the samples **PB**, **Mn3-Mn32%**, **MnFe** and **Mn^{2+}/PB**

Sample	$\nu(C\equiv N)$ (cm^{-1})	Size (nm)	Weight loss* (%)	ζ-potential (mV)
PB	2082	81±14	28.6	-38.8±6.52
Mn3%	2081	78±15	27.2	-46.8±8.43
Mn10%	2080	73±11	27.5	-37.5±5.81
Mn16%	2073	74±14	28.5	-42.9±5.67
Mn21%	2073	82±18	30.2	-35.1±6.25
Mn27%	2070	80±16	27.6	-39.5±5.06
Mn32%	2069	76±14	30.3	-32.8±5.28
MnFe	2068	64±12	30.6	-40.0±5.59
Mn^{2+}/PB	2082	69±11	34.6	-28.1±4.46

*Determined by TGA analysis

Table S2. Experimental and calculated χT values for some selected samples taking the presence of Mn^{2+} ions.

Sample	Measured $\chi T_{300\,K}$ ($cm^3\ K\ mol^{-1}$)	Calculated χT, ($cm^3\ K\ mol^{-1}$)
PB	4.432	4.375
Mn10%	4.327	4.375
Mn20%	4.292	4.375
Mn^{2+}/PB	4.721	4.900

In order to confirm the presence of Mn^{2+}, the χT values have been measured by using SQUID-MPMS magnetometer at room temperature (300 K) for four selected samples and compared them with the

calculated ones (Mn^{2+} (S=5/2), Fe^{3+} (S = 5/2), Fe^{2+} (S = 0)). Table S2 shows that the experimental values match well with the calculated ones confirming the presence of Mn^{2+} ions in samples, while a large discrepancy appeared between the experimental and calculated values taking an hypothesis of the presence of Mn^{3+} instead of Mn^{2+}.

Table S3. Lattice parameter calculated from the XRD patterns.

Sample	Lattice parameter (Å)
PB	10.1592(4)
Mn3%	10.163(1)
Mn10%	10.196(1)
Mn16%	10.226(1)
Mn21%	10.2192(3)
Mn27%	10.2311(4)
Mn32%	10.228(2)

Table S4. Energy of the configurations calculated by force-field based geometry optimization for Mn^{2+}-containing PB nanoparticles according to the different investigated scenario

Scenario	Energy (kcal mol^{-1})
Substitution of Fe^{3+} by Mn^{2+}	-23
Substitution of Fe^{3+} by Mn^{2+} coupled with the remove of $1Na^{+}$	-1
Substitution of 4 Fe^{3+} by 4 Mn^{2+} coupled with the remove of 1 $Fe(CN)_6^{4-}$	-86 (for 15% of substitution) and -93.5 (for 30% of substitution)

Table S5. Manganese release experiments for **Mn10%**, **Mn21%**, **Mn27%** and **Mn32%**

Sample	Na/Mn/Fe EDS ratios (after synthesis)	Mn/(Na-Mn-Fe)	Na/Mn/Fe EDS ratios (after 48 days in solution)	Mn/(Na-Mn-Fe)	% Mn release
Mn10%	11.87/10.30/77.83	10.3	12.5/9.75/77.75	9.75	-5.3
Mn21%	11.06/21.54/67.40	21.54	10.96/20.07/68.97	20.07	-6.8
Mn27%	13.21/26.85/59.94	26.85	11.48/25.51/62.48	25.51	-5.0
Mn32%	11.31/31.63/57.06	31.63	12.25/30.30/57.45	30.30	-4.2

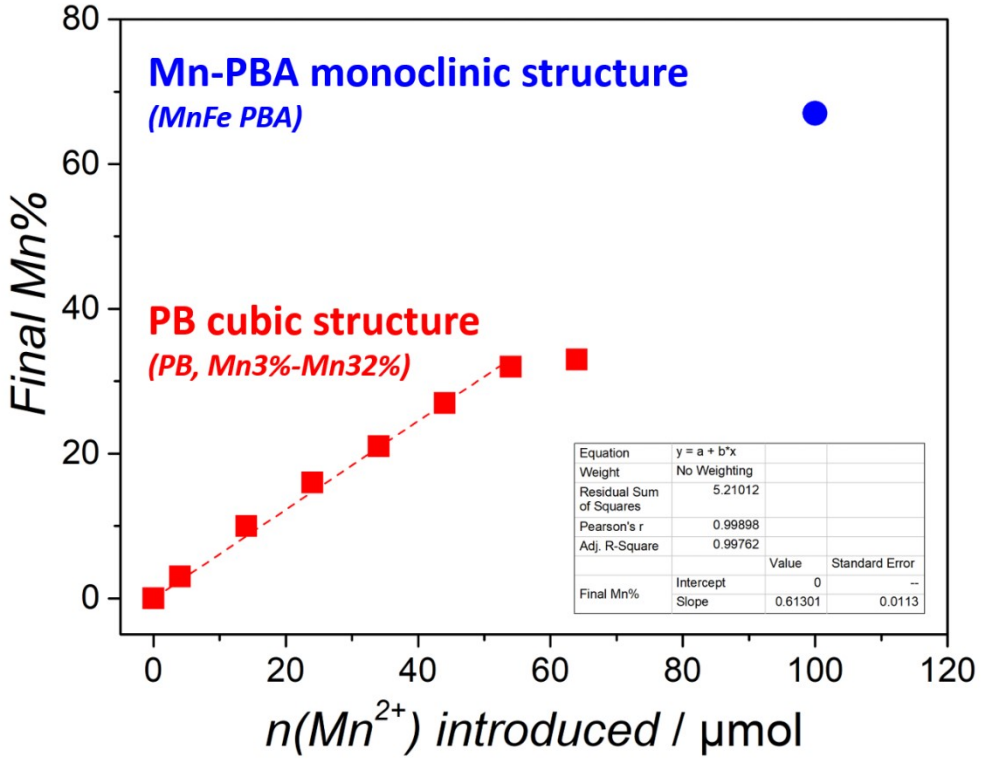

Figure S1. Inserted manganese amount (%) as a function of the initial Mn^{2+} concentration. A linear relation corresponds to a series of PB doped with Mn^{2+} compounds (from 0 to 32% of Mn^{2+}) presenting a conventional PB cubic structure (red points). The modification of the structure from cubic to monoclinic is observed with higher initial concentration of Mn^{2+} introduced during the synthesis. Sample with 70 % of Mn^{2+} (blue point) corresponds to $Mn[Fe(CN)_6]_{0.49}\square_{0.51}\cdot 3.2\ H_2O$ analogue (see after).[1]

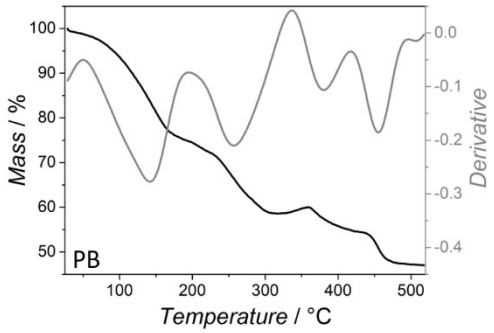
PB
Mass / %
Derivative
Temperature / °C

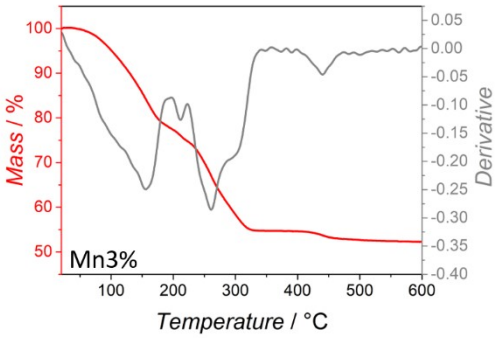
Mn3%
Mass / %
Derivative
Temperature / °C

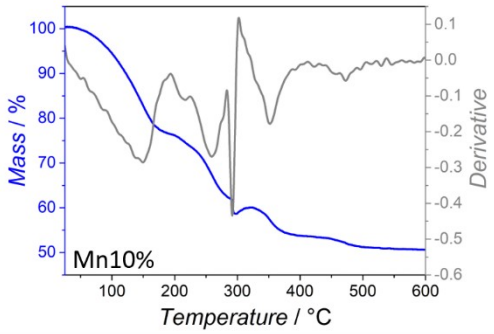
Mn10%
Mass / %
Derivative
Temperature / °C

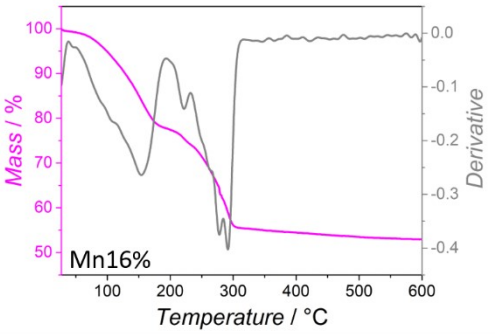
Mn16%
Mass / %
Derivative
Temperature / °C

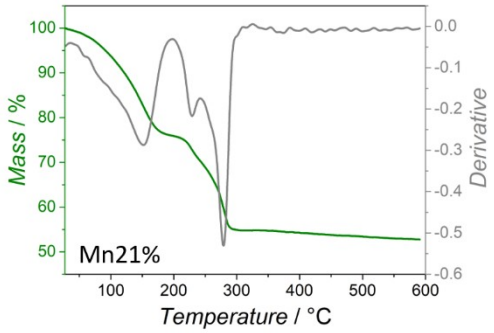
Mn21%
Mass / %
Derivative
Temperature / °C

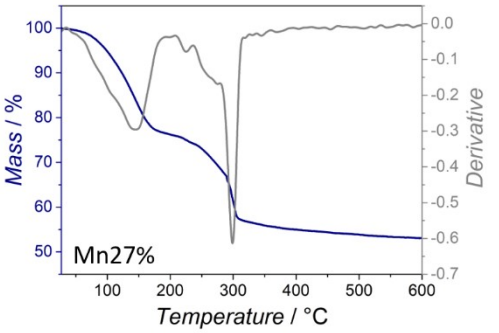
Mn27%
Mass / %
Derivative
Temperature / °C

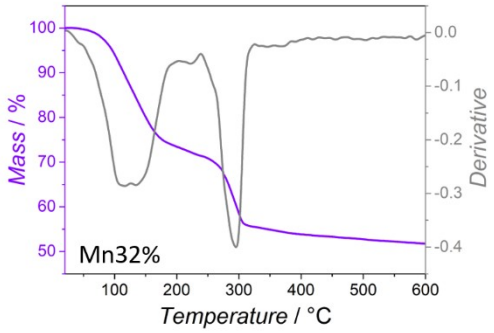
Mn32%
Mass / %
Derivative
Temperature / °C

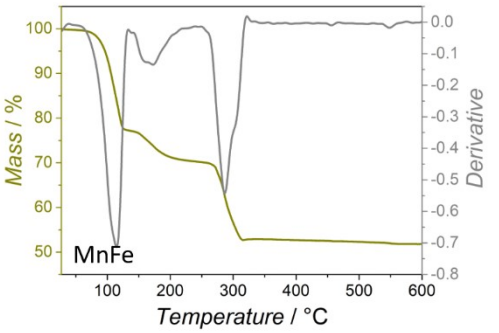
MnFe
Mass / %
Derivative
Temperature / °C

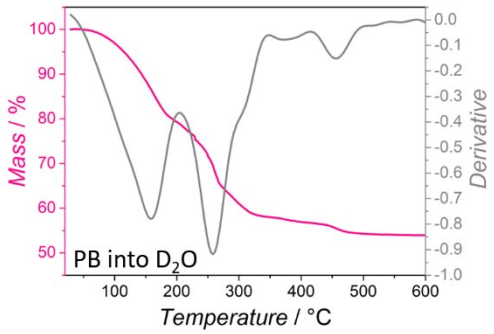
PB into D2O
Mass / %
Derivative
Temperature / °C

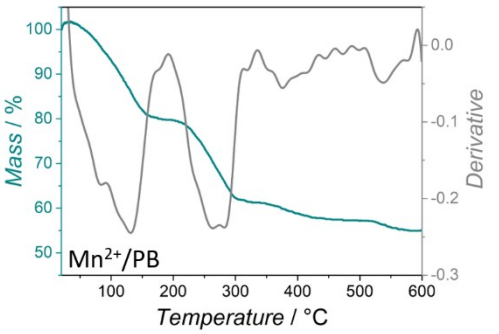
Mn2+/PB
Mass / %
Derivative
Temperature / °C

Figure S2. TGA curves for investigated samples **PB**, **Mn3-32%**, **MnFe** and **Mn^{2+}/PB**.

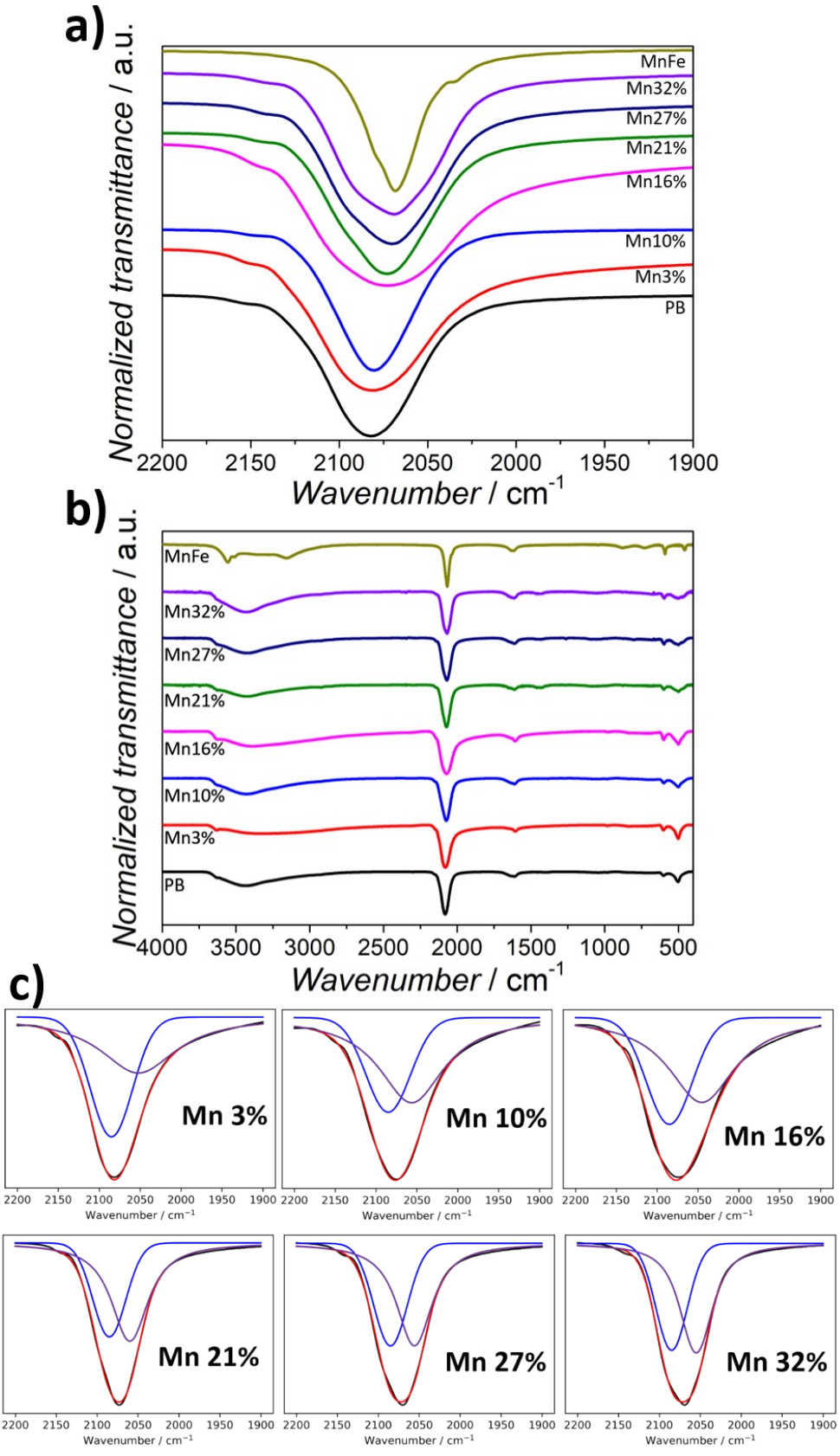

Figure S3. a) FTIR spectra for **PB**, **Mn3-32%** and **MnFe**; b) Magnification of the FTIR spectra in the cyanide stretching vibration 1900 – 2200 cm^{-1} region for **PB**, **Mn3-32%** and **MnFe**; c) Deconvolution

of peaks in the cyanide stretching vibration in the 1900 – 2200 cm^{-1} region for Mn^{2+}-containing PB nanoparticles showing the presence of two components at 2082 and 2068 cm^{-1}.

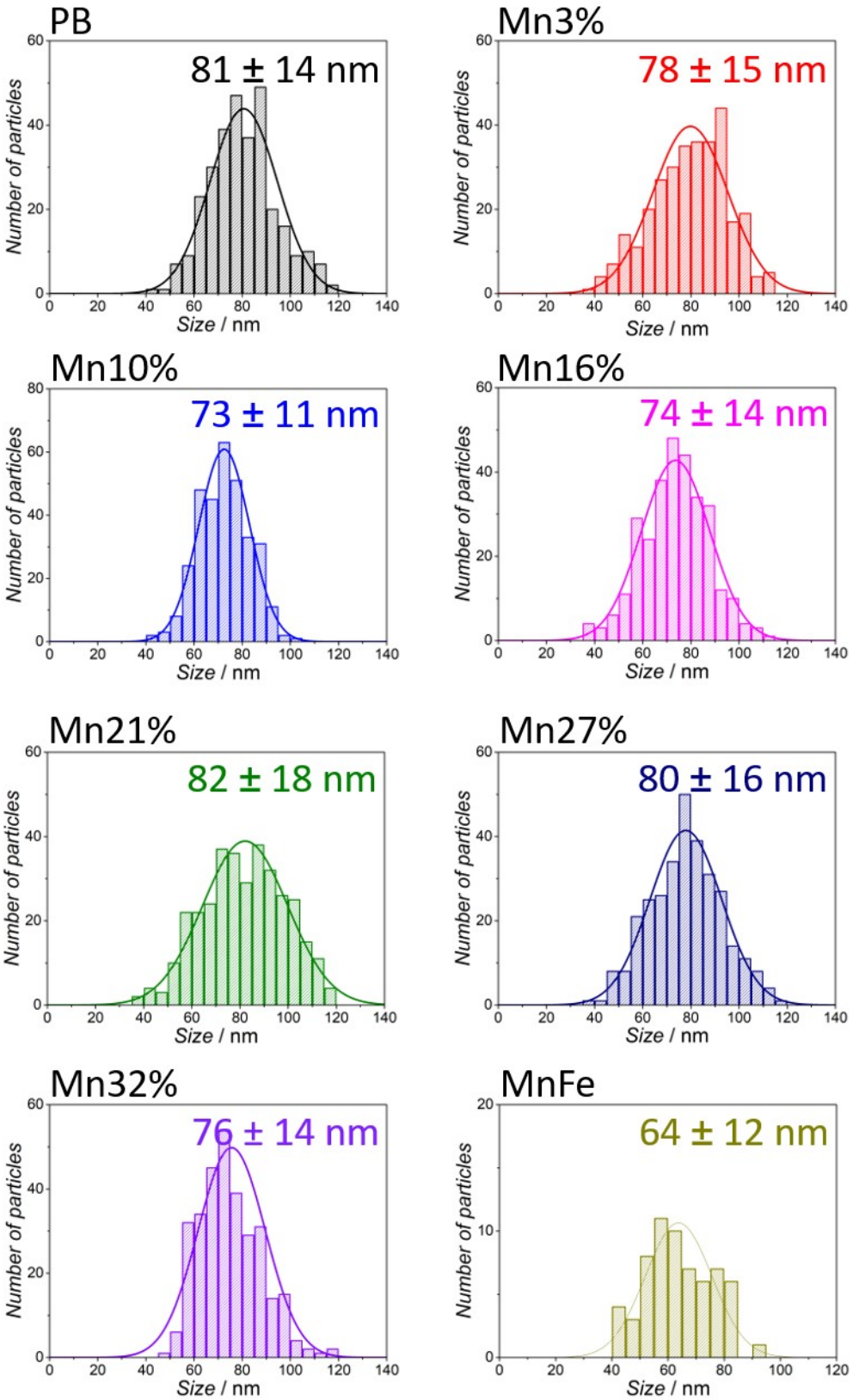

Figure S4. Size distribution histograms of **PB**, **Mn3-32%** and **MnFe**.

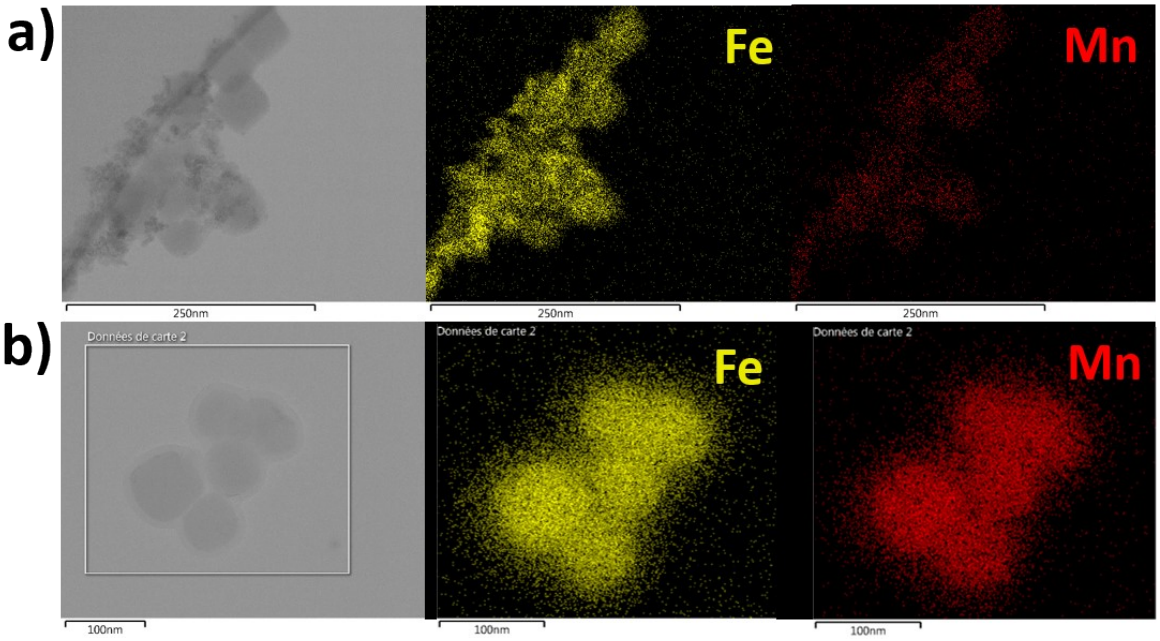

Figure S5. STEM images of: a) **Mn10%** and b) **Mn32%** and the corresponding STEM-energy dispersive spectrometer elemental mapping of iron (yellow) and manganese (red).

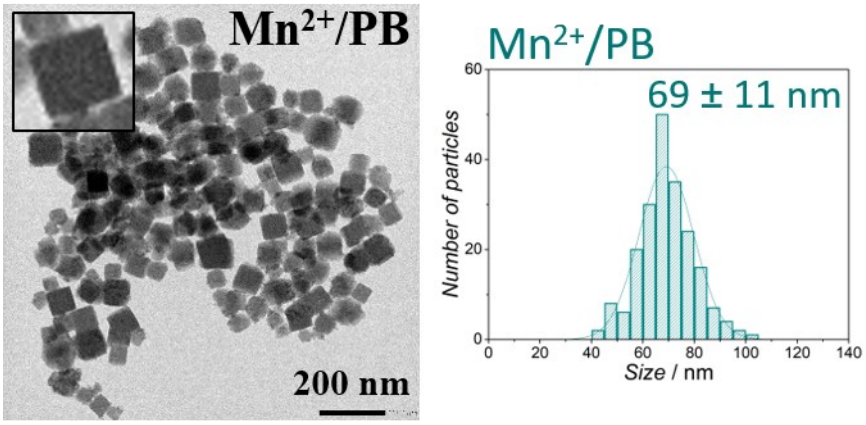

Figure S6. TEM image of **Mn^{2+}/PB** nanoparticles obtained by post-synthetic insertion of Mn^{2+} ions into PB network and its size distribution histogram.

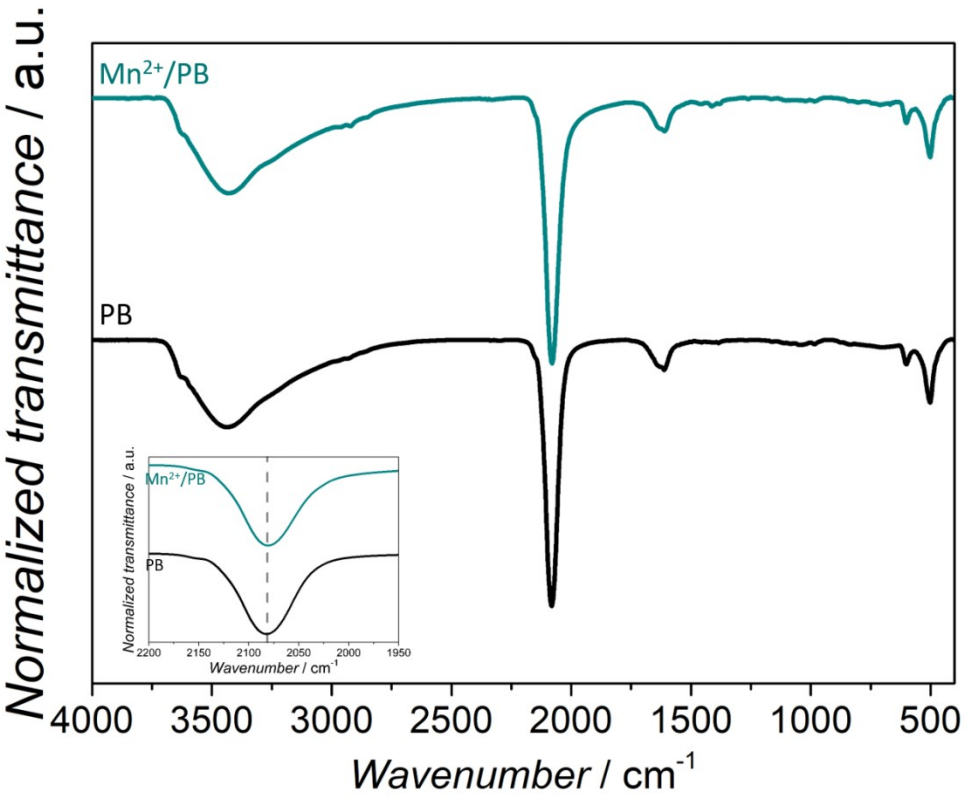

Figure S7. IR spectra for **Mn^{2+}/PB** nanoparticles obtained by **the** post-synthetic insertion of Mn^{2+} ions and the pristine PB nanoparticles. Inset: Magnification of the IR spectra in the cyanide group stretching window (2200 – 1950 cm^{-1}).

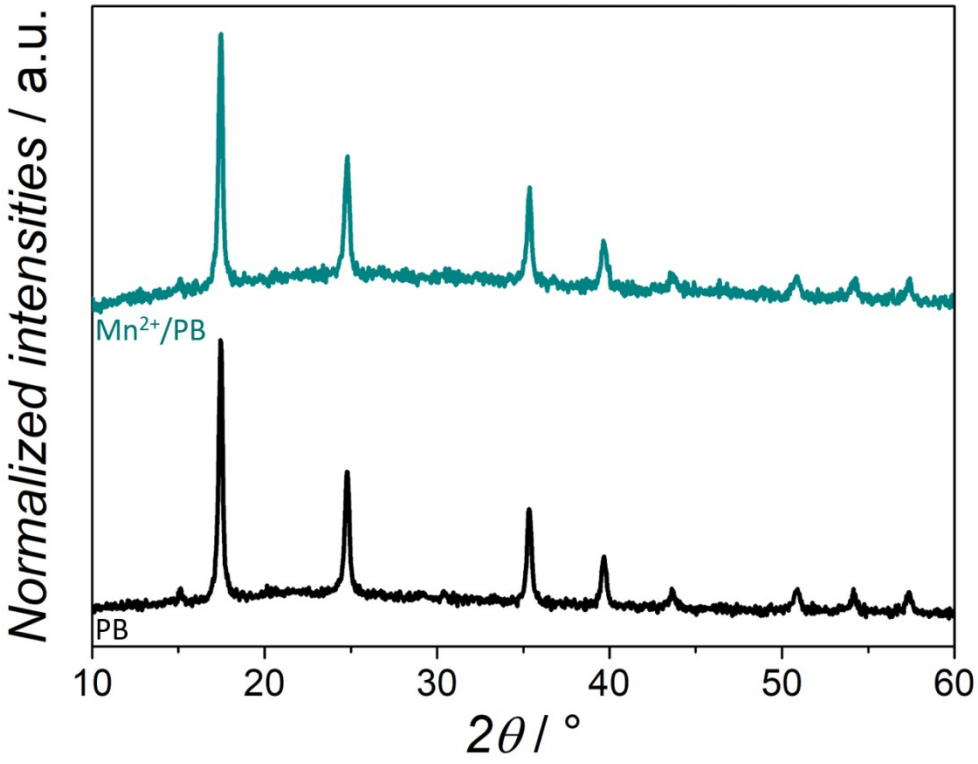

Figure S8. PXRD pattern of **Mn^{2+}/PB** nanoparticles obtained by post-synthetic insertion of Mn^{2+} into PB network and comparison with the PXRD pattern of the pristine PB nanoparticles.

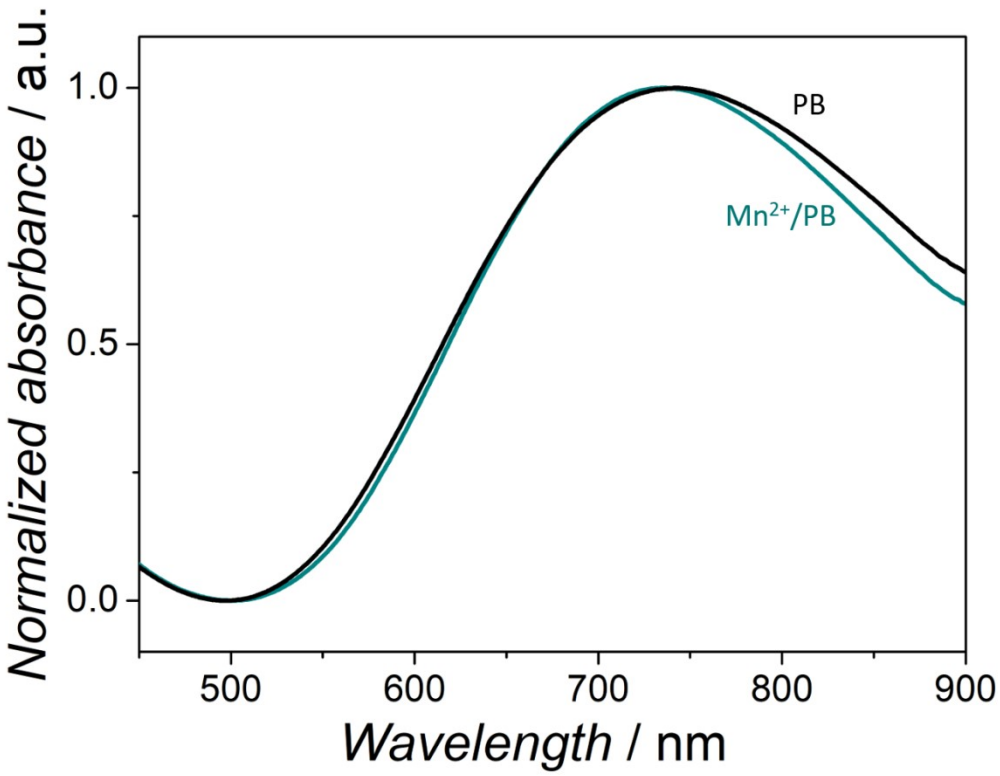

Figure S9. Electronic spectra in the visible region for **Mn^{2+}/PB** and **PB** nanoparticles in water.

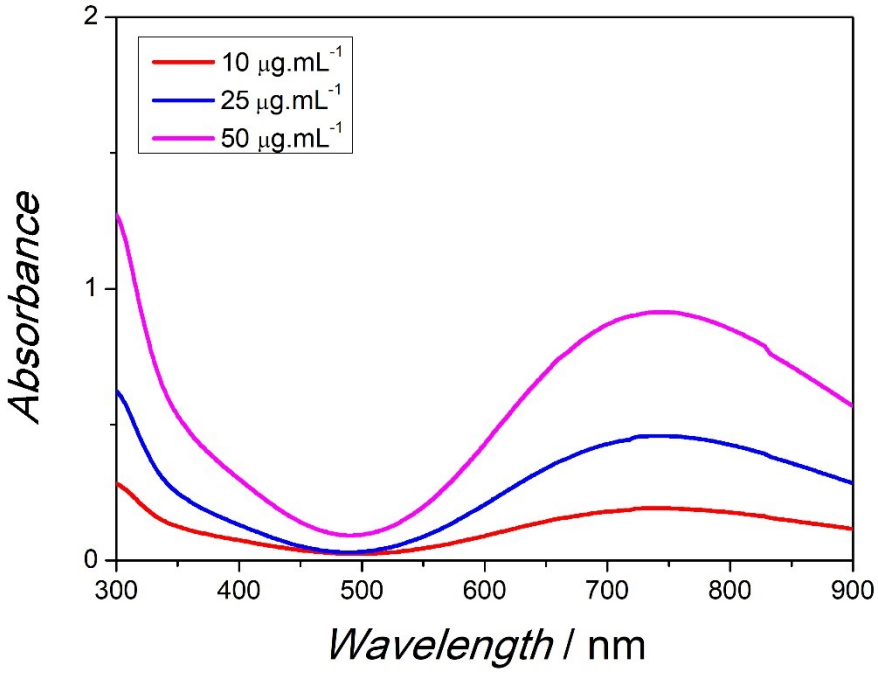

Figure S10. Absorption of aqueous suspensions at different concentrations for **PB** sample.

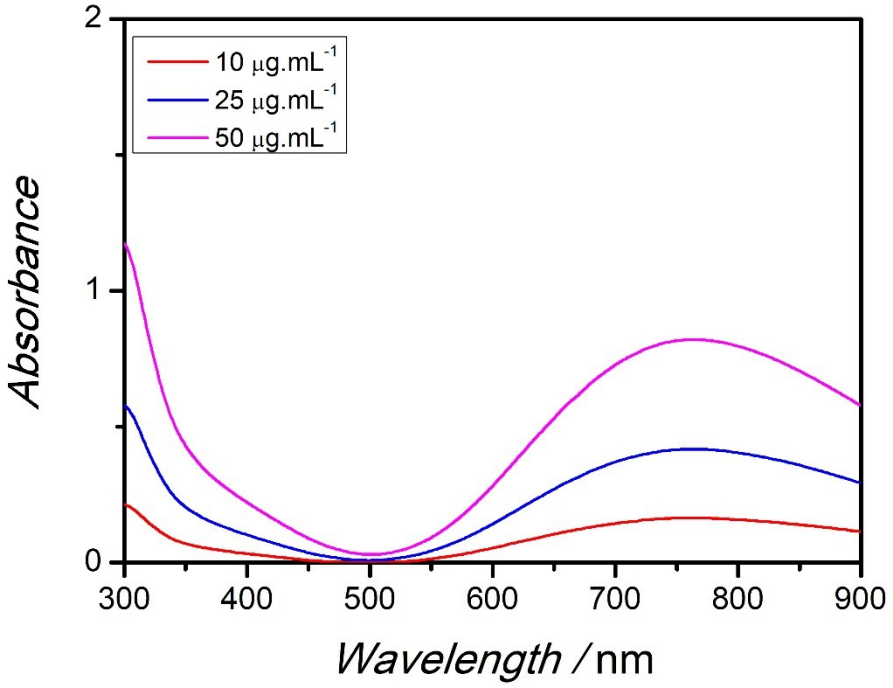

Figure S11. Absorption of aqueous suspensions at different concentrations for **Mn10%**.

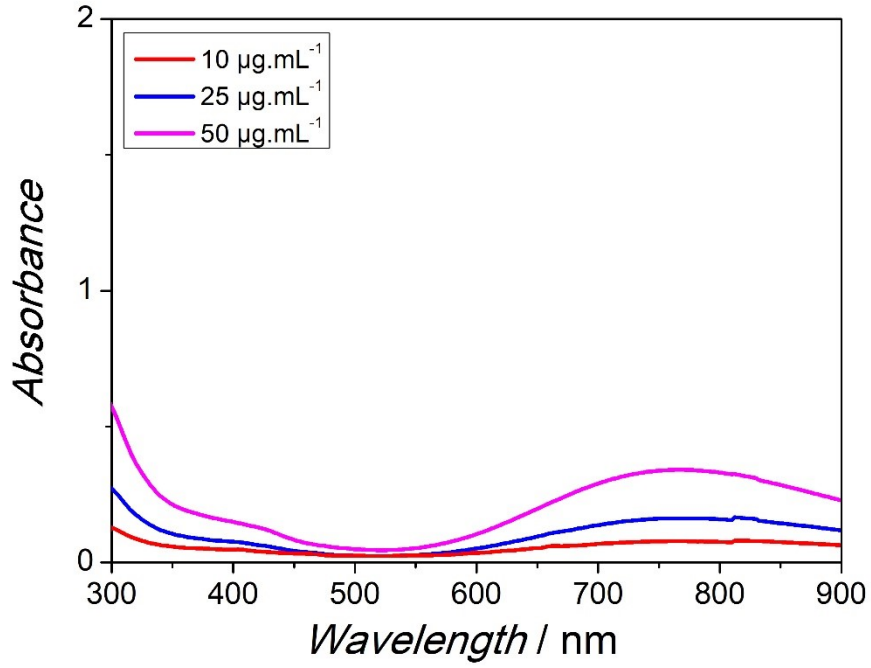

Figure S12. Absorption of aqueous suspensions at different concentrations for **Mn27%**.

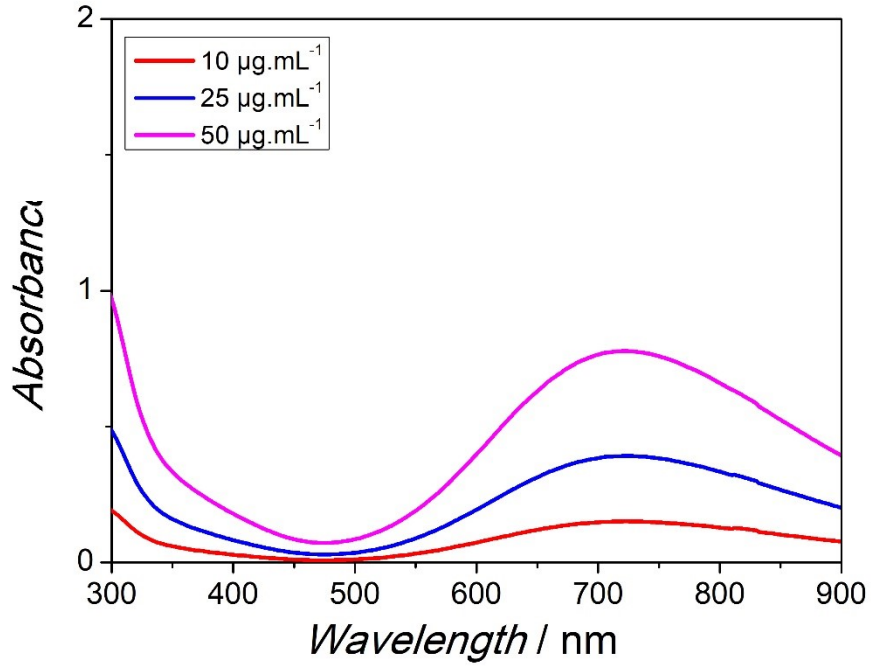

Figure S13. Absorption of aqueous suspensions at different concentrations for **PB** nanoparticles synthetized into **D_2O**.

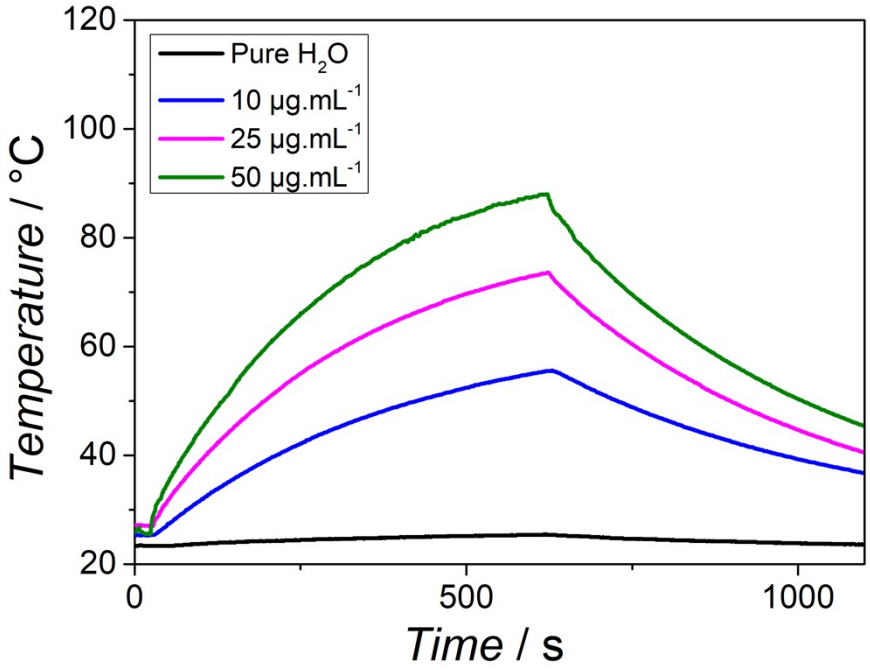

Figure S14. Photothermal activity of **PB NPs** suspensions at various concentrations in water (10 min irradiation 3 W cm^{-2} + 10 min laser OFF).

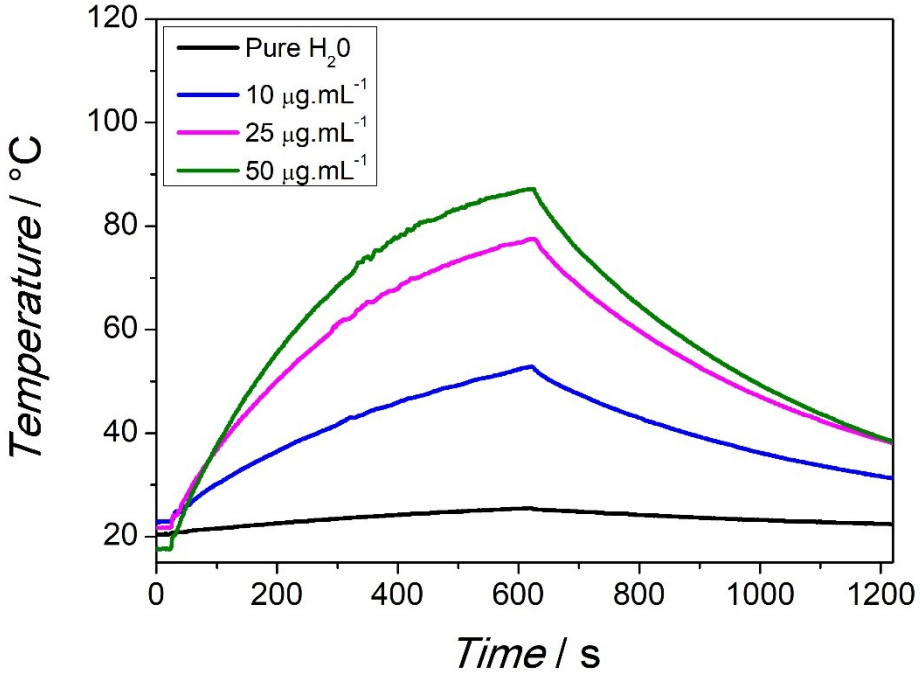

Figure S15. Photothermal activity of **Mn10% NPs** suspensions at various concentrations in water (10 min irradiation 3 W cm^{-2} + 10 min laser OFF).

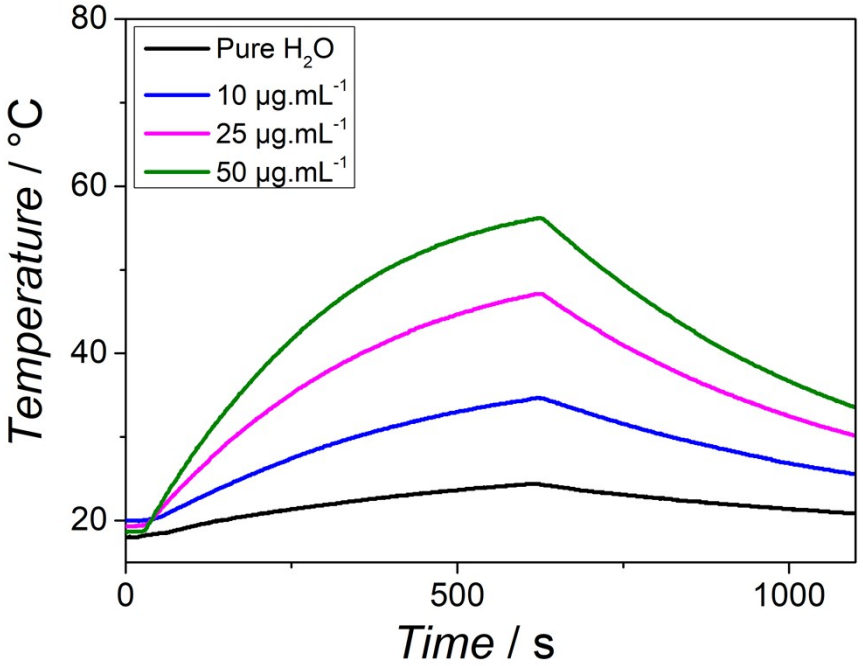

Figure S16. Photothermal activity of **Mn27% NPs** suspensions at various concentrations in water (10 min irradiation 3 W cm^{-2} + 10 min laser OFF).

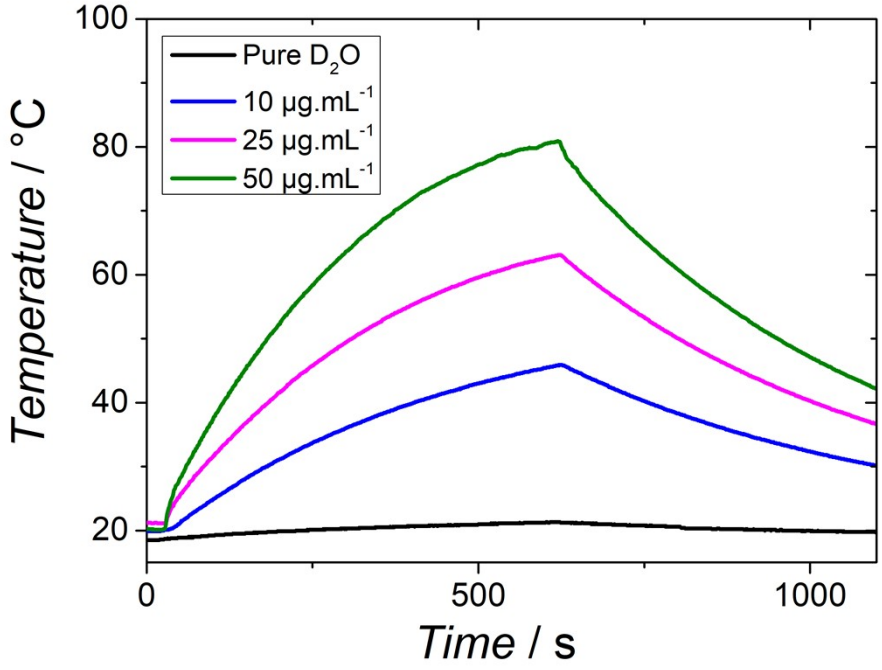

Figure S17. Photothermal activity of **PB NPs synthetized into D_2O** suspensions at various concentrations in D_2O (10 min irradiation 3 W cm^{-2} + 10 min laser OFF).

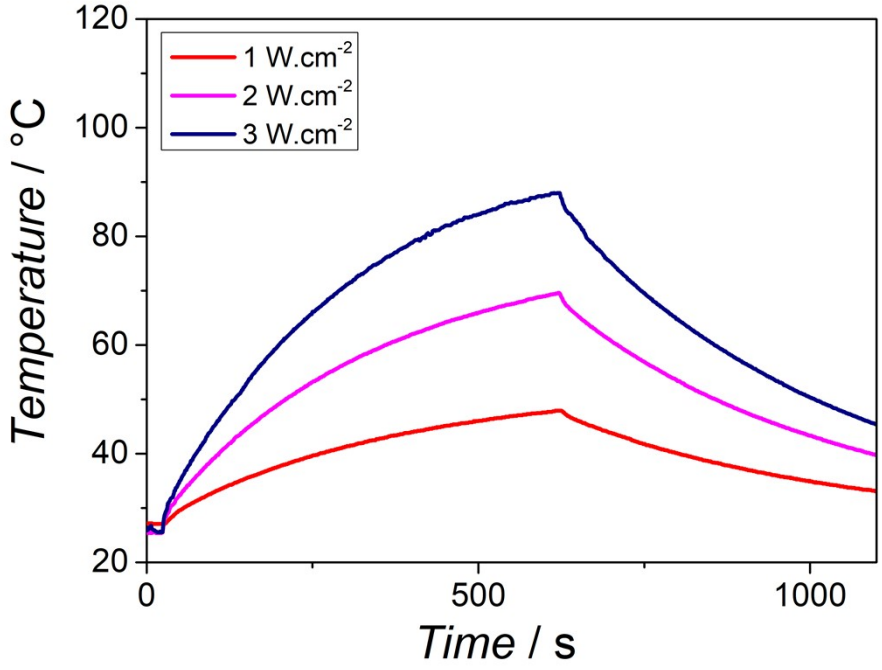

Figure S18. Temperature elevation of **PB NPs** suspension at 50 µg mL^{-1} concentration in water measured after 10 min irradiation at various laser power densities + 10 min laser OFF.

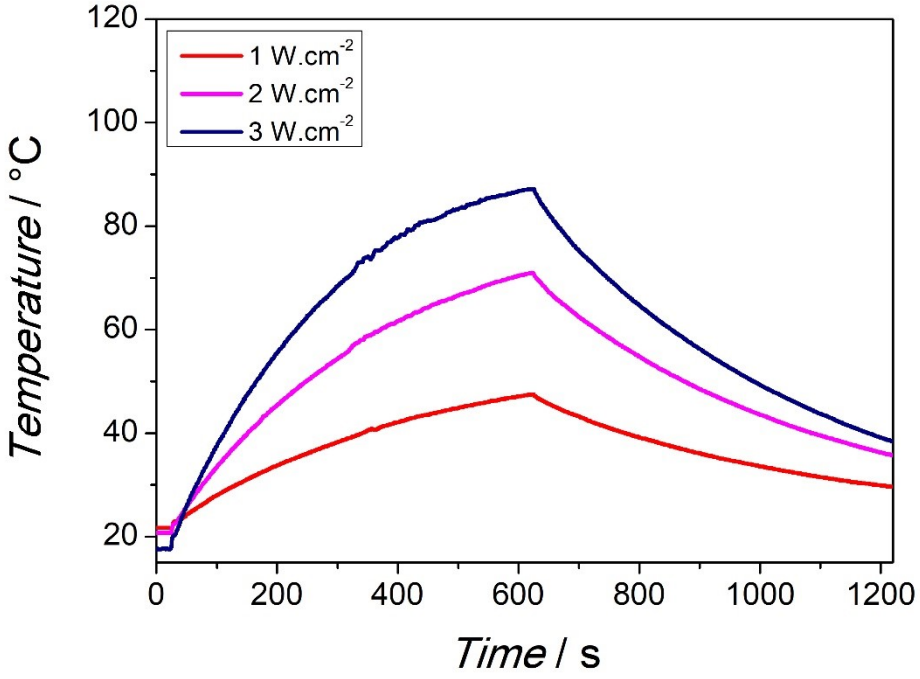

Figure S19. Temperature elevation of **Mn10% NPs** suspension at 50 µg mL^{-1} concentration in water measured after 10 min irradiation at various laser power densities + 10 min laser OFF.

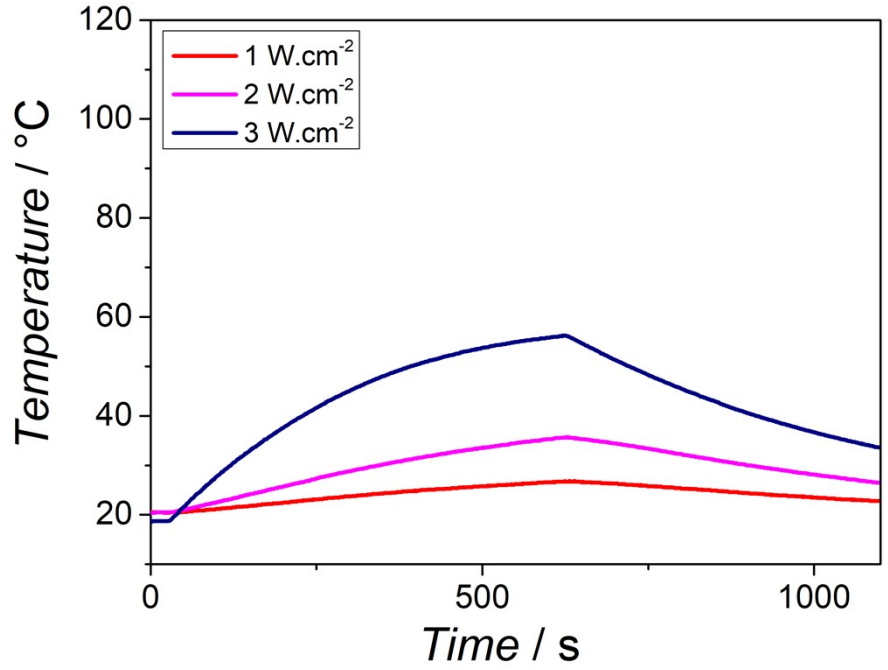

Figure S20. Temperature elevation of **Mn27% NPs** suspension at 50 µg mL^{-1} concentration in water measured after 10 min irradiation at various laser power densities + 10 min laser OFF.

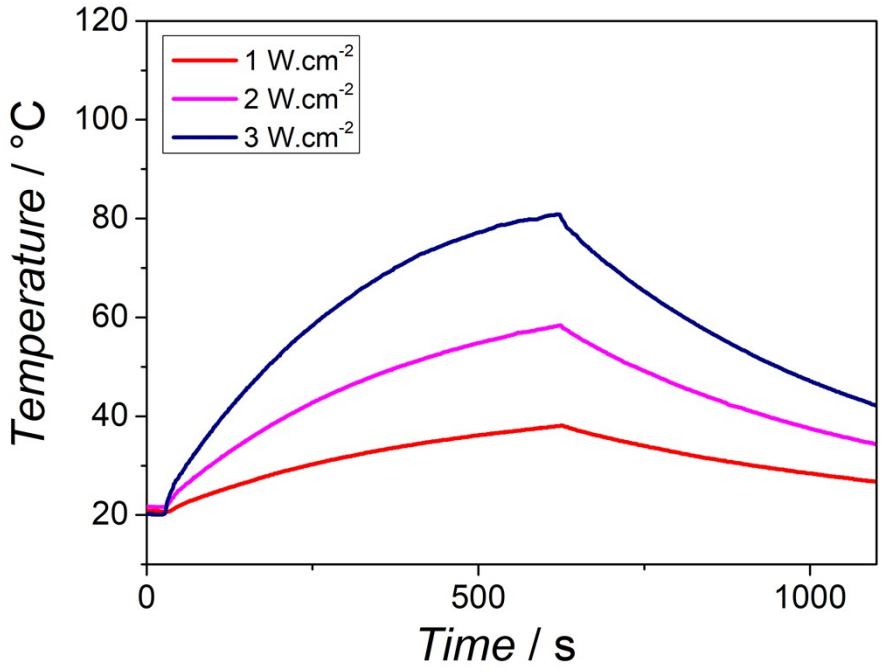

Figure S21. Temperature elevation of a suspension of **PB NPs synthetized into D_2O** in D_2O at 50 µg mL^{-1} concentration measured after 10 min irradiation at various laser power densities + 10 min laser OFF.

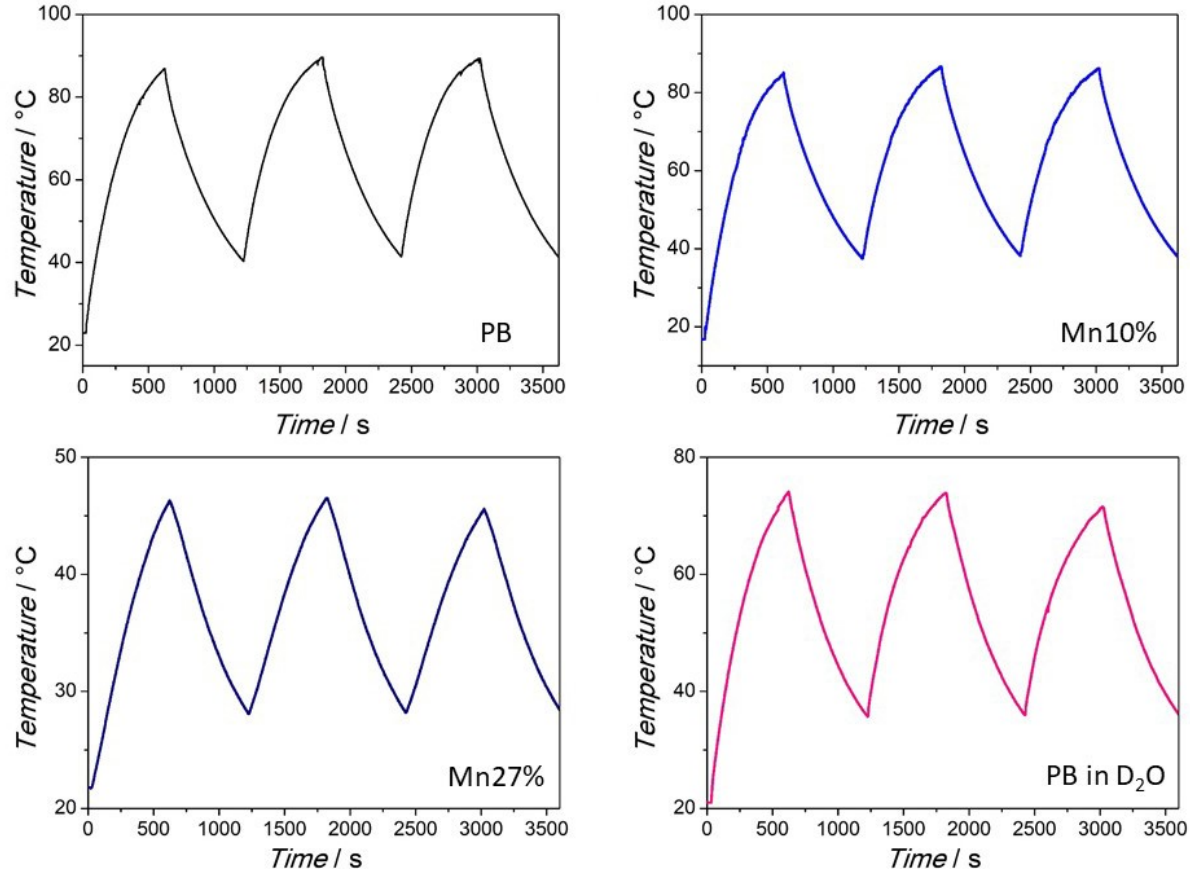

Figure S22. Stability measurement of **PB NPs, Mn10%, Mn27%** suspensions in water and of **PB into D_2O** in D_2O at 50 µg mL^{-1} by three heating cycles under 808 nm laser irradiation (3 W cm^{-2}). For practical reasons linked with the recording capacity of the thermometer, manual laser activation etc. the cooling time was fixed at 10 min.

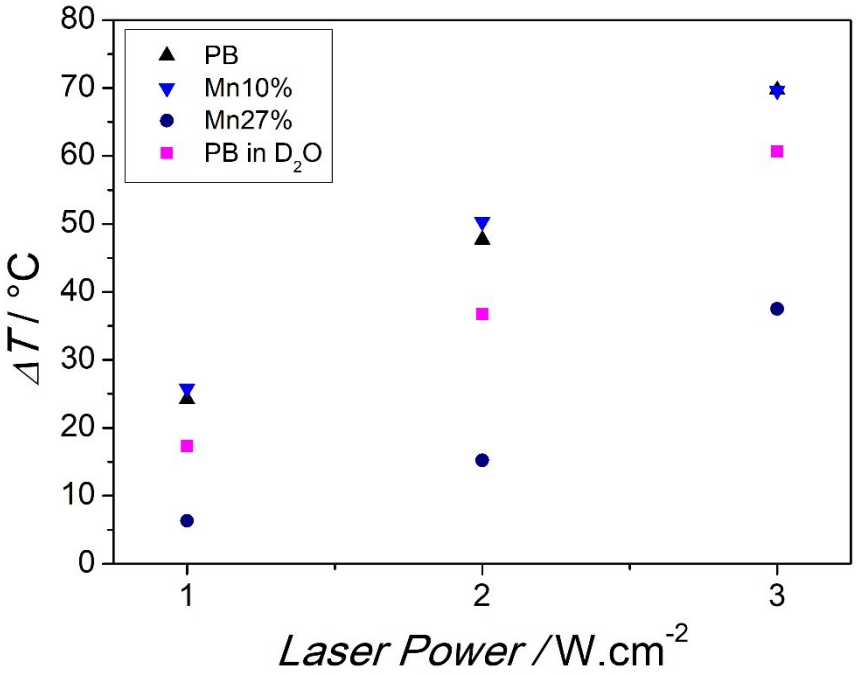

Figure S23. Temperature elevations measured at various laser power at 808 nm and under 10 min laser irradiation for all the compounds: **PB** (black), **Mn10%** (blue), **Mn27%** (navy) in water and, **PB synthetized into D_2O** in D_2O (magenta) at 50 µg mL^{-1} concentration.

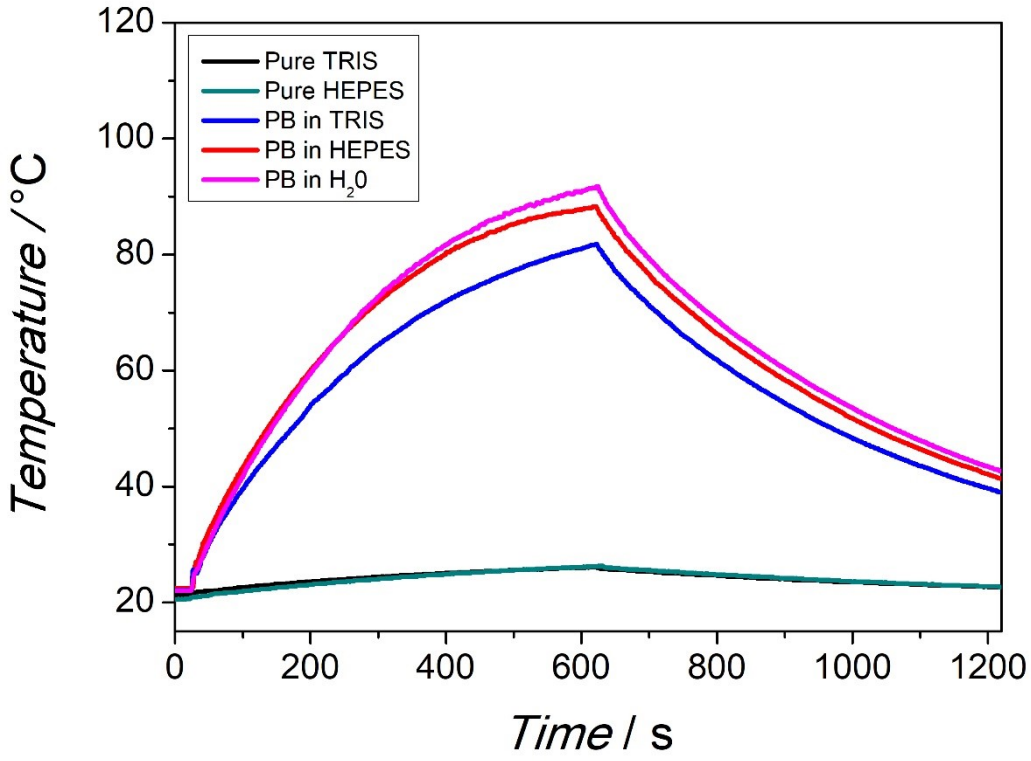

Figure S24. Temperature elevation of a suspension of **PB NPs** in HEPES (1M, PH = 7.5) and in TRIS (1M, PH = 7.2) buffers at 50 µg mL^{-1} concentration measured after 10 min irradiation at various laser power densities + 10 min laser OFF.

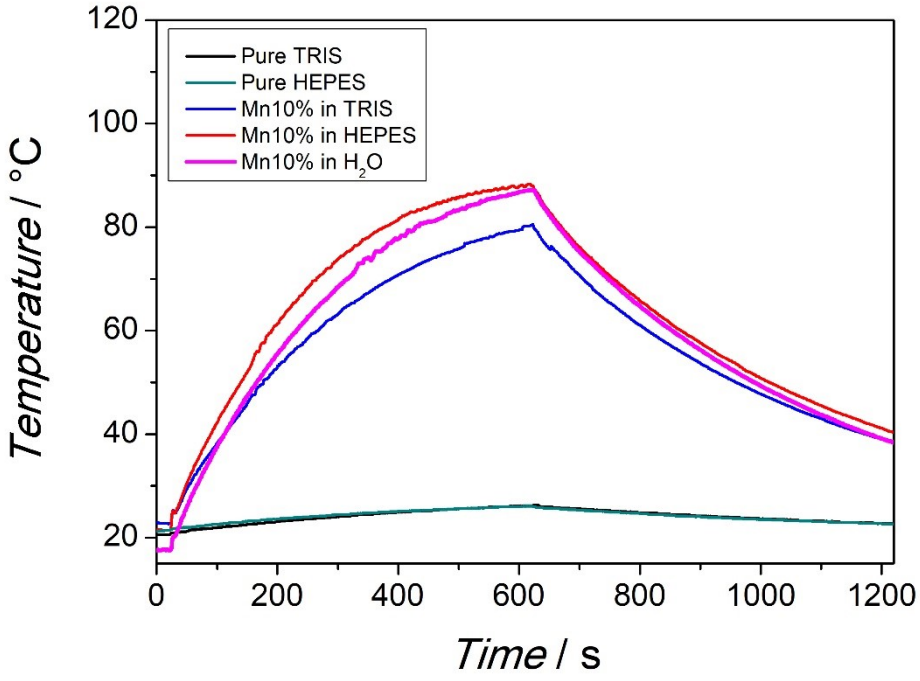

Figure S25. Temperature elevation of a suspension of **Mn10% NPs** in HEPES (1M, PH = 7.5) and in TRIS (1M, PH = 7.2) buffers at 50 µg mL^{-1} concentration measured after 10 min irradiation at various laser power densities + 10 min laser OFF.

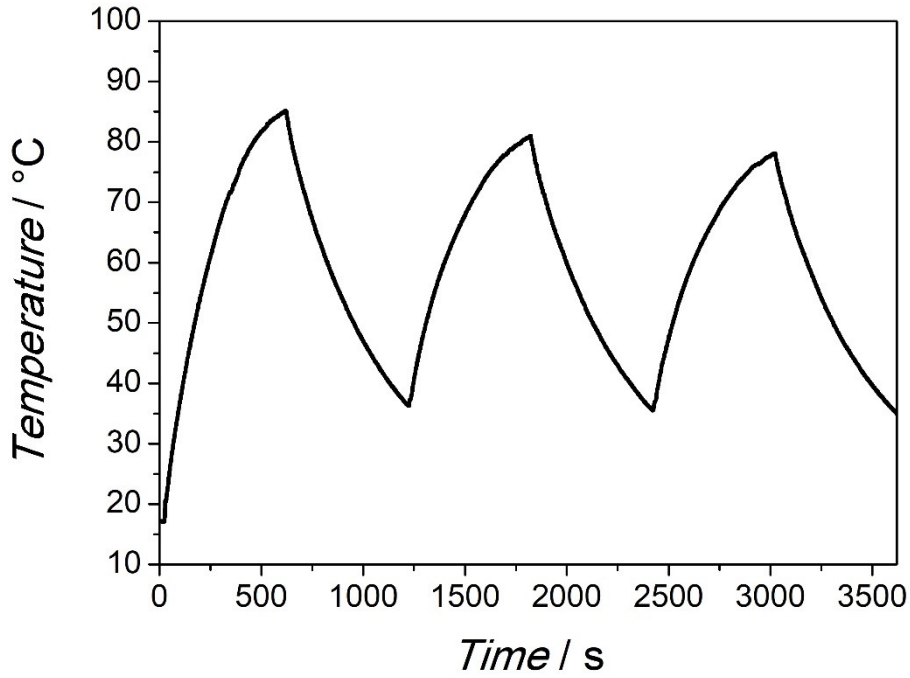

Figure S26. Stability measurement of **Mn10%** suspensions in HEPES (1M, PH = 7.5) at 50 µg mL^{-1} by three heating cycles under 808 nm laser irradiation (3 W cm^{-2}).

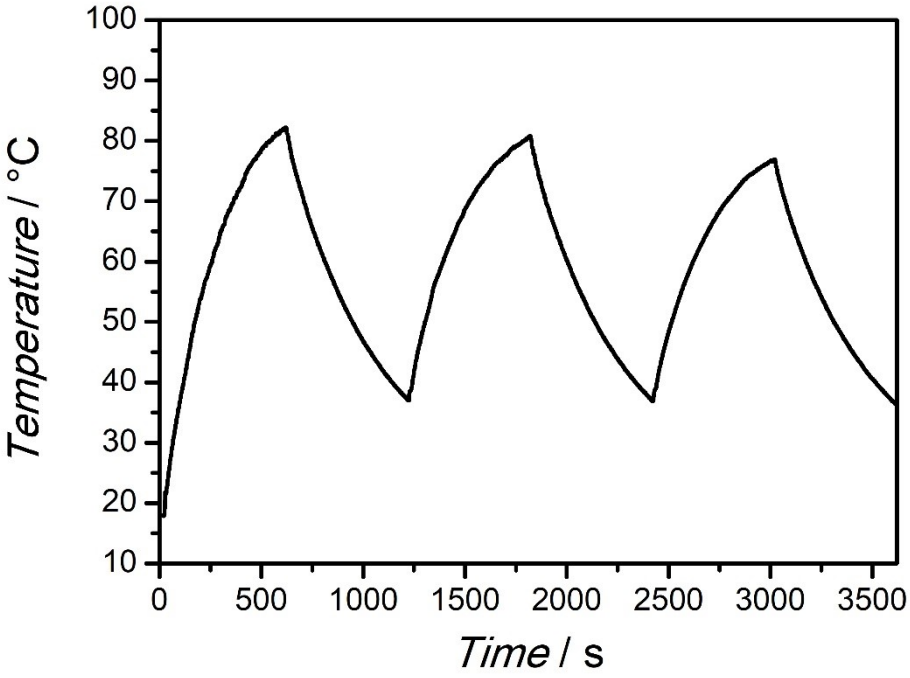

Figure S27. Stability measurement of **Mn10%** suspensions in HEPES (1M, PH = 7.5) at 50 µg mL^{-1} by three heating cycles under 808 nm laser irradiation (3 W cm^{-2}).

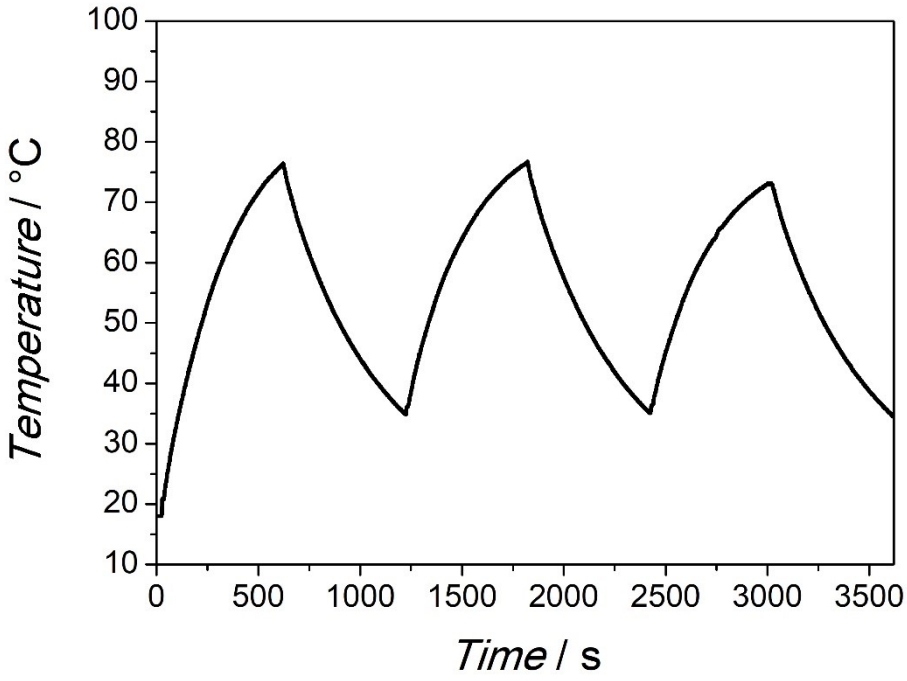

Figure S28. Stability measurement of **Mn10%** suspensions in TRIS (1M, PH = 7.5) at 50 µg mL^{-1} by three heating cycles under 808 nm laser irradiation (3 W cm^{-2}).

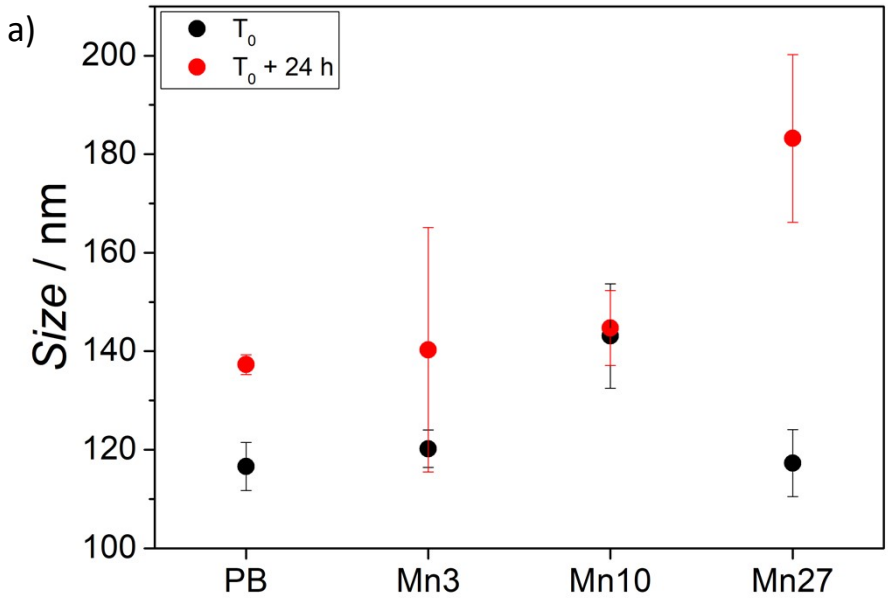

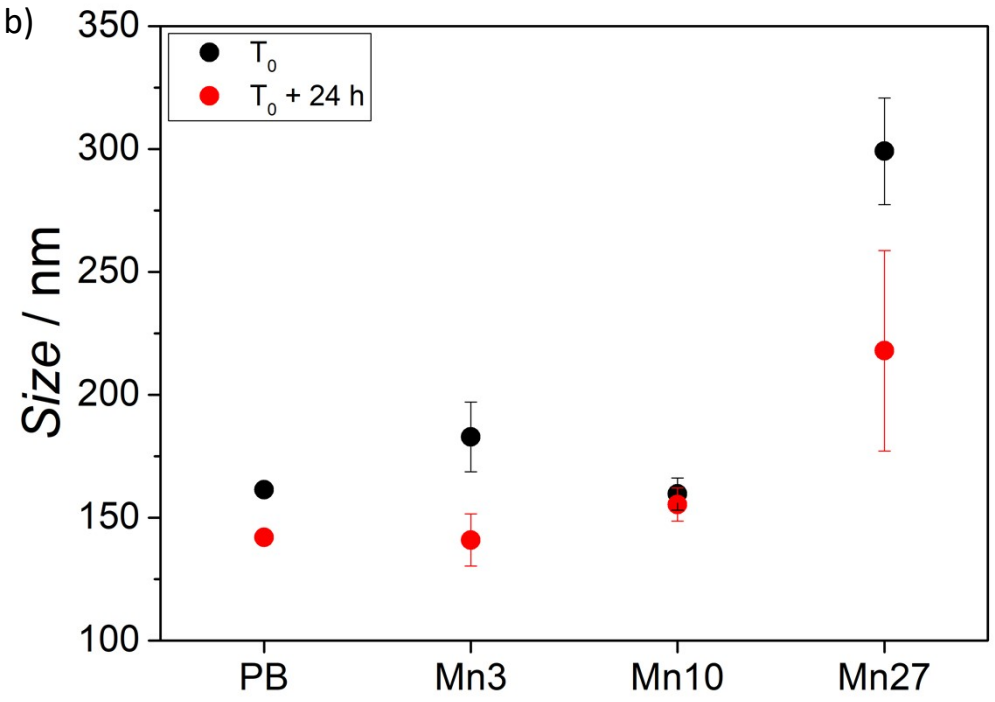

Figure S29. Hydrodynamic radius of **PB**, **Mn3%, Mn10%** and **Mn27%** nanoparticles suspensions in PBS buffer (pH = 7) (a) and in solution containing 5% of glucose usually used for *in-vivo* injections involving zebrafish (b) performed by Nanoparticle tracking analysis technique.

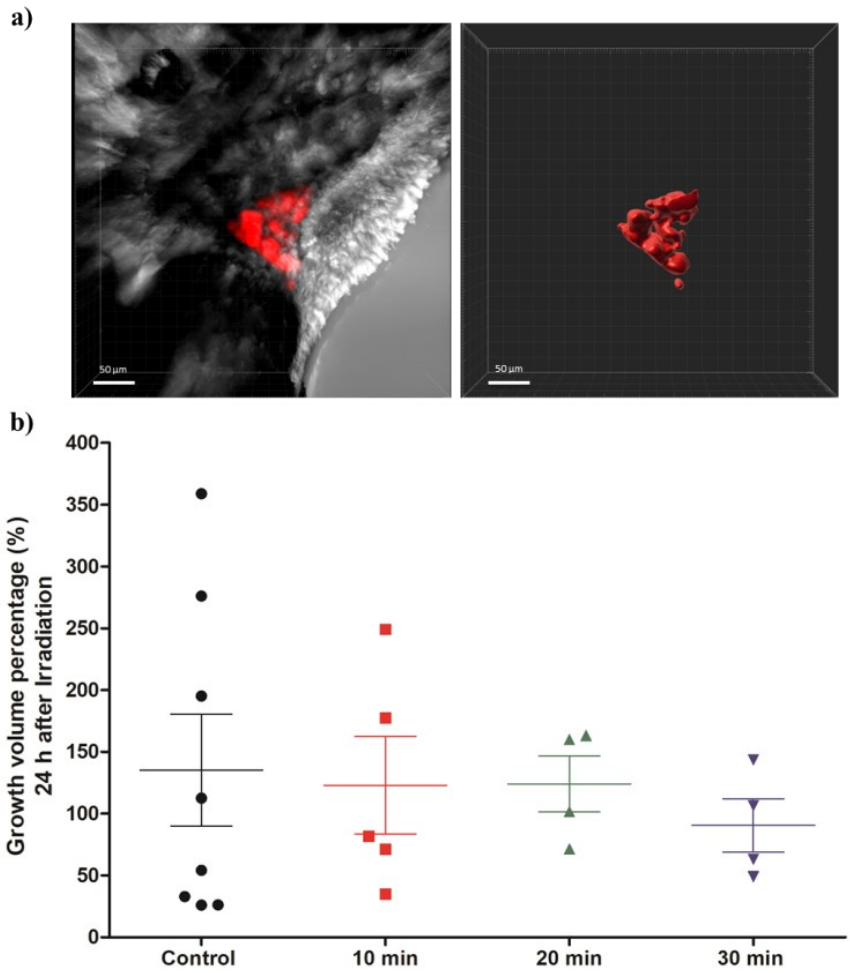

Figure S30. Photothermal therapy effect of Mn10% nanoparticles *in vivo* under continuous laser irradiation. a) Reconstructed 3D images of **Mn10%** nanoparticles treated MDA-MB-231-LUC-RFP xenograft in Casper zebrafish embryos using Imaris software, in order to calculate the xenograft volumes in μm^3. b) The xenograft growth volume percentage (%) of each embryo 24 h after irradiation at 808 nm (2.5 W cm^{-2}) for 10, 20 and 30 min. Control is embryos injected with cells and not exposed to irradiation. Each point represents an embryo.

[1] Gómez, A., Lara, V., Bosch, P., Reguera, E., *Powder Diffraction*, 2002, **17(2)**, 144-148.